

Study of the Reaction $\pi^+n \rightarrow p\pi^0\pi^0$ at 2.1 GeV/c

K. J. Braun* and D. B. Cline

University of Wisconsin, Madison, Wisconsin 53706

(Received 13 July 1972; revised manuscript received 20 April 1973)

Using the reaction $\pi^+d \rightarrow pp$ (MM) at 2.13 GeV/c with photons from the final-state π^0 's detected by tantalum plates in the 30-in. ANL bubble chamber, a $2\pi^0$ mass spectrum has been obtained in several ways. This spectrum is found to be in good agreement with phase-space expectations and presents no evidence for the production of a "narrow" ϵ ($\Gamma < 200$ MeV). The $2\pi^0$ cross section for $\Delta^2 < 15\mu^2$ is $386 \pm 80 \mu\text{b}$. $\pi\pi$ production and scattering angular distributions are presented. Good agreement with the one-pion-exchange model is noted. Assuming that the ratios of peripheral pion-production cross sections are equal to their pole values, a new method for extracting $\pi\pi$ scattering parameters is discussed. Using this method the $I = 0$ s -wave phase shift is uniquely determined from threshold to 1 GeV/c² and found to be similar to the so-called UP-DOWN solutions of s - p wave interference analyses. In addition, the ratios of $I = 0$ to $I = 2$ s -wave scattering phase shifts and scattering lengths are found to be equal to $-(3.2_{-1.0}^{+1.5})$ near $\pi\pi$ threshold. Using a dispersion sum rule, the $\pi\pi$ scattering lengths are found to be $a_0 = +(0.15 \pm 0.08)\mu^{-1}$ and $a_2 = -(0.05 \pm 0.01)\mu^{-1}$.

I. INTRODUCTION

This experiment was performed at the Argonne National Laboratory by exposing the 30-in. bubble chamber (B.C.) filled with deuterium to a separated π^+ beam of three incident momenta around 2.2 GeV/c.¹ Tantalum plates were installed in the chamber to act as photon converters. In this paper events with two final-state protons, identified by ionization, and their associated photons are used to analyze the reaction

$$\pi^+n \rightarrow p\pi^0\pi^0. \quad (1)$$

Motivation for studying (1) centers on interest in the s -wave interaction of the reaction

$$\pi^+\pi^- \rightarrow \pi^0\pi^0 \quad (2)$$

which is of great theoretical importance as one of the simplest and most basic examples of the strong interaction. Bose statistics restrict the $2\pi^0$ system to even orbital angular momentum states. Reaction (2) should, therefore, be very suitable for studying the s -wave interaction, at least in the energy range where higher partial waves can safely be ignored. This is especially true since complications due to the p -wave resonance, the ρ , cannot arise. Since free pion targets are unfortunately not available, information about (2) must be inferred from data on (1), usually via the one-pion exchange (OPE) model.² This indirect approach vastly complicates the problem. It was the primary purpose of this investigation to provide data which might be useful for the study of reaction (2).

To extract the $2\pi^0$ final state from the experi-

mentally observed reaction

$$\pi^+d \rightarrow pp(\text{MM}), \quad (3)$$

three techniques have been used:

1. Events with very small momentum transfer t have been selected. t is the momentum transfer from target neutron to final-state proton in units of pion masses squared.³
2. The contribution from the production of η , ω , η' , $3\pi^0$, and $\Delta^+(1236)$ has been subtracted.
3. The sample with two or more γ rays has been used to kinematically fit to a $2\pi^0$ hypothesis.

Section II deals with certain preliminaries such as data reduction, the deuteron target, Monte Carlo simulation, and the method used to obtain cross sections. Section III describes the techniques used in obtaining the $2\pi^0$ spectrum and Sec. IV contains our experimental results. In Sec. V we describe our method for deducing phase-shift information on reaction (2) and present our results.

II. PRELIMINARIES

A. Beam and Target

Table I shows the beam momentum distribution resulting from the three magnet settings. From beam profile curves and by counting δ rays⁴ the proton contamination was judged to be less than 1%. A scale schematic diagram of the target bubble chamber showing the location of the tantalum plates is given in Fig. 1.

B. Scanning and Measuring

The film was scanned for those topologies containing either one or two final-state protons,

TABLE I. Experimental information.

| | 1st setting | 2nd setting | 3rd setting |
|--|--------------|--------------|--------------|
| Beam (GeV/c) | 2.04 ± 0.011 | 2.17 ± 0.011 | 2.33 ± 0.014 |
| No. of pictures | 75 000 | 40 000 | 31 000 |
| No. of tracks/frame ^a | 18.1 | 14.9 | 18.1 |
| Mean beam value (GeV/c) | | 2.13 | |
| c.m. energy (GeV) | | 2.21 ± 0.09 | |
| Radiation length of 1 Ta plate | | 0.76 | |
| B field in B.C. (kG) | | 32.53 | |
| D ₂ density (g/cm ³) ^a | | 0.135 | |
| B.C. interaction length (cm) | | 55 | |

^a Reference 4.

identified by ionization. In addition, for each event a search was made for associated photons converted in the Ta plates. To reject unassociated γ 's, an event vertex had to be within a cone $\pm 4^\circ$ about the bisector of a symmetric pair of conversion electrons. Templates and pointers were used to assist the scanners in proton identification and γ -vertex association. Finally, one person edited the entire 2-prong scan, making sure all γ 's were found and properly associated and only definitely identified protons appeared in the final state. The shorter or darker of the protons in the 2-prong sample was defined as the spectator proton. The effective recoil-proton momentum cutoff (scan cutoff) was determined by comparing the 3- and 4-prong data in this film⁵ with those of Ref. 6. It is ~ 1.25 GeV/c.

The resulting events were measured on the Wis-

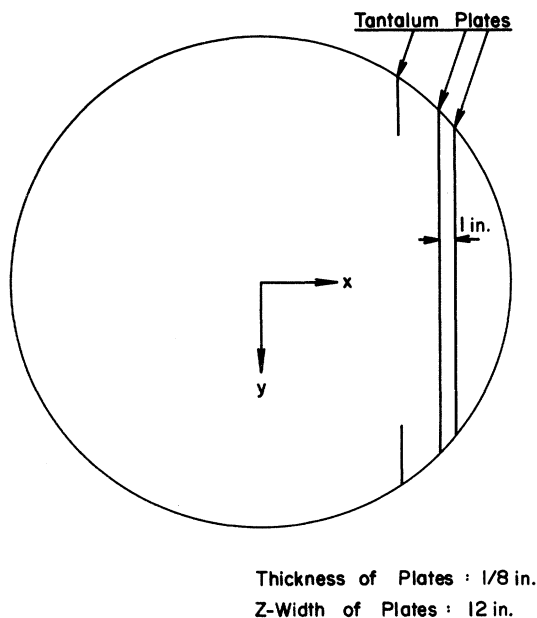


FIG. 1. 30-in. bubble-chamber scale schematic diagram.

TABLE II. Yields after kinematic fitting.

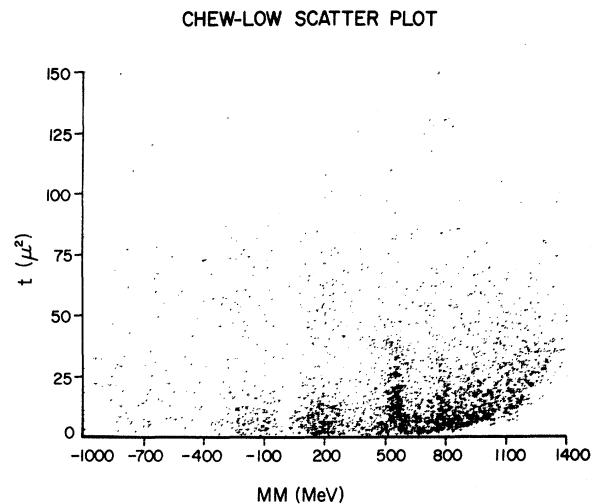
| | 0 γ | 1 γ | 2 γ | 3 γ | 4 γ | Total |
|-------------------------------|------------|------------|------------|------------|------------|-------|
| 1-prong events, no editing | 1039 | 1402 | 843 | 233 | 68 | 3585 |
| 2-prong events, after editing | 613 | 1055 | 860 | 250 | 95 | 2873 |

consin image-plane digitizers (one-prong events) and film-plane microscopes (two-prong events).

C. Fitting

All events were passed through the Wisconsin reconstruction-fitting program DIANA-HASH.^{7a} A fiducial volume was imposed essentially restricting event vertices to the volume starting 3 cm upstream of the first Ta plate. In addition, in the 2-prong sample, the spectator had to have a momentum less than 0.3 GeV/c. A 2-constraint (2-C) fit to the 2 γ sample revealed no significant correlation between the photon energy obtained from the fitting program and that found in the scan. Thus, the possibility of using the scan γ -energy estimates as input to our fitting programs was rejected. The events for all three beam momenta were lumped together and are distributed among the different topologies as shown in Table II. Figures 2 and 3 show the Chew-Low plot and mass projections for the two-prong events.

Events with two or more γ 's were then processed by TVGP-SQUAW^{7b} to test the special 2 π^0 hypotheses to be discussed shortly. The resolution turned out to be so poor for the one-prong events that very little information could be gained from that sample. All results to be presented will, therefore, be based on the two-prong events.

FIG. 2. Chew-Low plot of (missing mass) vs t for $\pi^+n \rightarrow p + (\text{MM})$.

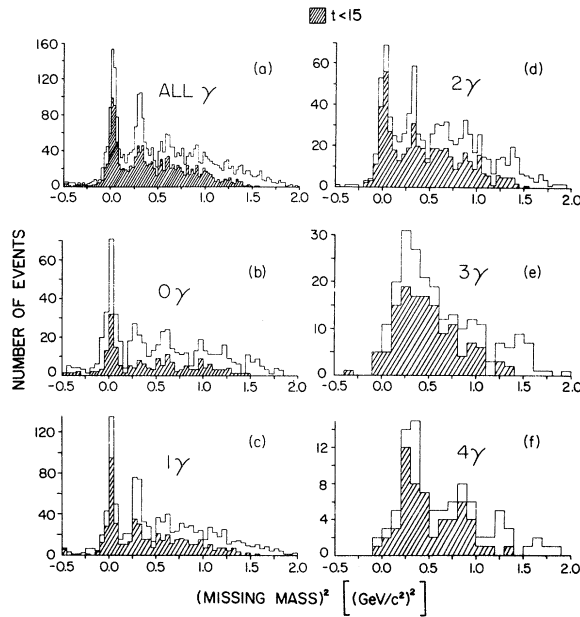
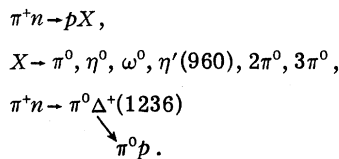


FIG. 3. Raw missing-mass-squared distributions, with (shaded) and without t cuts, for (a) all two-prong events and (b)–(f) broken down into 0γ – 4γ samples. t refers to the momentum transfer from target neutron to final-state proton in units of pion mass squared (μ^2).

In order to obtain an enriched $2\pi^0$ sample and to permit background estimates and the determination of $\pi^0\pi^0$ angular distributions, events with two or more γ 's were fitted to the $2\pi^0$ final-state hypothesis. For the 4γ sample this implies a straightforward 2-C fit. The minimum-opening-angle approximation is necessary to fit the 2γ and 3γ samples.^{1d, 8} Two cases are possible in the 2γ case. First, both visible γ 's originate from the same π^0 , and, second, one γ from each π^0 is detected. The above procedure, checked and tuned with Monte Carlo calculations, made it possible to cut down the $3\pi^0$ background by a factor of ~ 2 and to obtain an independent estimate of $\Delta^+(1236)$ production.

D. Monte Carlo Simulation

In order to study background and obtain detection and fitting efficiencies the program FAKE⁹ was used to generate events of the following types:



These events received spatial and beam momentum distributions to simulate the vertex and c.m. energy distributions of the actual events. The various reactions were given the production and

decay angular distributions shown in Fig. 4^{5, 8, 10–13} and Ref. 14.

Programs were added to FAKE to determine if (1) a γ was detected geometrically, (2) a γ converted in the plates, and (3) the resultant electron-positron pair emerged from the plates. To answer (2) and (3), the shower curves of Crawford and Messel¹² shown in Fig. 4(c) were used. The average number of e^+ emerging after an E -GeV photon traverses x radiation lengths of tantalum was assumed to be proportional to the photon detection efficiency. The normalization was provided by assuming that above 1 GeV the detection efficiency is given by the

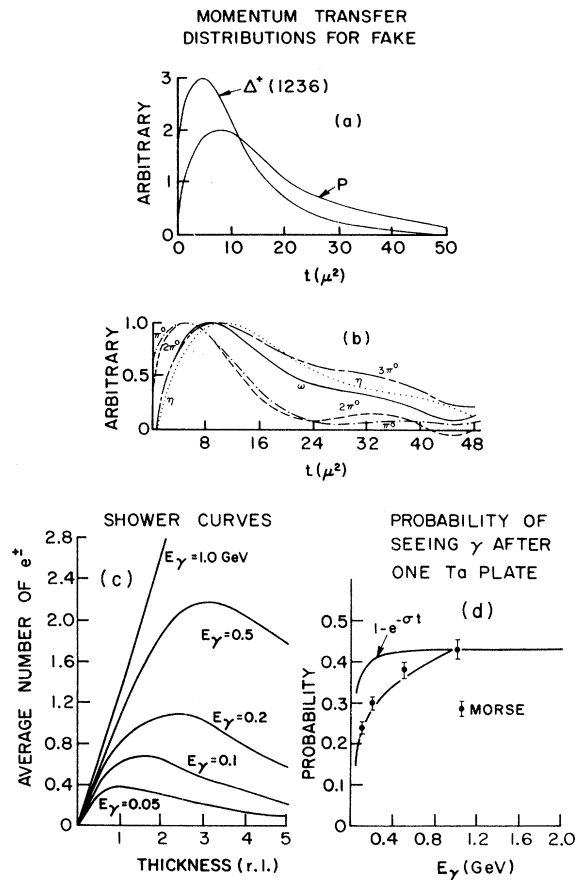


FIG. 4. (a) FAKE input for Δ^+ production (Ref. 11). More sharply peaked distribution is momentum transfer calculated from target nucleon to final-state $\Delta^+(1236)$. Broader distribution was obtained by calculating t to the proton resulting from $\pi^+n \rightarrow \Delta^+\pi^0 \rightarrow p\pi^0\pi^0$. (b) Momentum-transfer distributions used as input for FAKE. The $2\pi^0$ and $3\pi^0$ distributions were assumed to be equal to those for $\pi^+\pi^-$ and $\pi^+\pi^-\pi^0$ from Ref. 5. The others came from Refs. 10 and 13. (c) Shower curves for lead (Ref. 12). (d) Probability that a photon of energy E_γ is detected after traversing one of tantalum plates in the bubble chamber. Upper curve is pair-production probability; data points are from Ref. 8a.

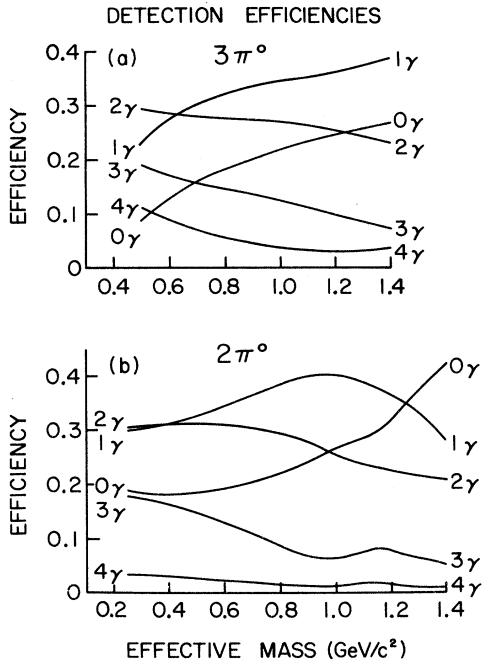


FIG. 5. FAKE γ -detection efficiencies for (a) 0γ – 4γ rays from the $3\pi^0$ final state; (b) same as (a) for $2\pi^0$.

pair-production probability. The resulting efficiency for one plate is shown in Fig. 4(d), where we also indicate Morse's⁸ results obtained from an experimental study of electrons incident on a Ta plate of the same thickness. Our procedure was checked against the experimentally observed charge-exchange detection efficiencies obtained from the π^0 peaks of Figs. 3(a)–3(d). The agreement was excellent. In Fig. 5 are shown the resulting $2\pi^0$ and $3\pi^0$ detection efficiencies.

Finally, FAKE assigned errors to the kinematic variables previously generated. The distributions of these errors, as well as of the kinematic variables themselves, closely matched the experimental ones. FAKE events were then processed by the same SQUAW fitting program used for the real events to enable us to study the fitting efficiencies for the various $2\pi^0$ hypotheses. The stretch and confidence-level distributions for real charge-exchange fits were used as checks on the FAKE results. Again, the agreement was good.

E. Cross-Section Determination

The cross sections in this experiment were obtained by normalizing to the charge-exchange channel. Since we are interested in "free" neutron cross sections, we would like a stationary neutron target. We actually observe interactions with bound neutrons. This leads to distortions of the observed production angular distributions due to

Fermi statistics at low t and the Fermi motion of the target at high t . Detailed model calculations are necessary to correct for these effects. The following procedure obviates the need for such detailed calculations.

Since the charge-exchange reaction



in hydrogen is charge-symmetric to the reaction



on a "free" neutron, and charge symmetry is a valid conservation law for strong interactions, the cross sections for reactions (4) and (5) are the same. In this experiment we observe the charge-exchange reaction



which is interpreted, using the spectator model, which was found to be valid,¹⁴ as the interaction of a π^+ with a *bound* neutron. A comparison of the experimental results for reaction (6) with published results for (4) thus provides a method for extracting "free" neutron cross sections from the observed channels in reaction (3).

In Fig. 6(a) the t distributions are shown for reactions (4) and (6) with our data normalized to those in hydrogen^{13, 15} in the interval $5\mu^2 < t < 40\mu^2$ where the cross sections are believed to be the same. This normalization yields a pathlength $P = 1.74 \pm 0.11$ events/ μb . Since the scattering amplitudes depend only on t and s , the total c.m. energy, scaling our data points by the factor in Fig. 6(c) maps the charge-exchange cross section in deuterium into that in hydrogen. Furthermore, since the different channels in reaction (3) are similarly affected by target motion to first order,¹⁶ their "free" neutron cross sections can be similarly determined. Thus, the differential cross section $d\sigma$ for *any* n - γ channel in reaction (3) can be written as

$$d\sigma = N \frac{d\sigma_4}{N_6} \frac{\epsilon_n}{\epsilon}, \quad (7)$$

where $d\sigma_4$ = differential cross section for reaction (4), N = number of $n\gamma$ events observed in the channel of interest, N_6 = number of $n\gamma$ events observed in channel (6), ϵ_n = efficiency for detecting n photons in channel (6), and ϵ = efficiency for detecting n photons in the channel under consideration. Of course, the ϵ 's are equal to unity if all γ samples are lumped together. If a momentum-transfer selection is made, Eq. (7) is integrated. In that case σ_4/N_6 is given by Fig. 6(b).

Similar procedures have been successfully used elsewhere.^{10, 17} In our case, it is possible to automatically correct for scanning losses at low and

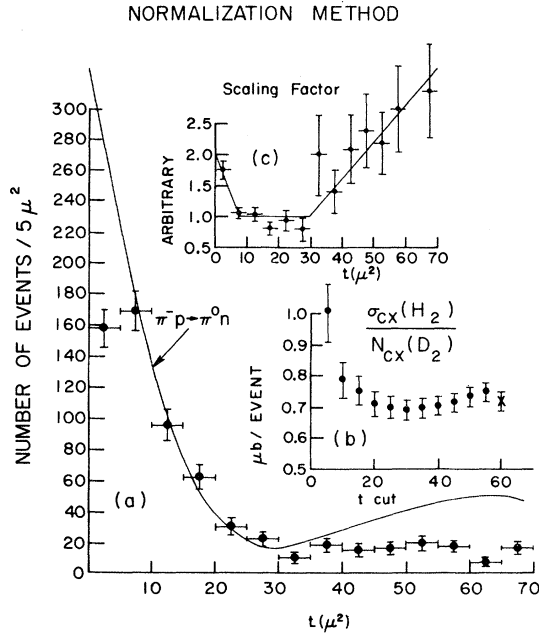


FIG. 6. (a) Charge-exchange momentum-transfer distribution. Obtained by counting events in π^0 peak symmetrically. Curve represents charge-exchange cross section in hydrogen from Refs. 13 and 15 averaged over our c.m. energy and normalized to $5\mu^2 < t < 40\mu^2$. (b) Normalization factor σ_i/N_6 for momentum-transfer selections. Point X is factor used when no t cut is made (scan cutoff). (c) Scaling factor. Obtained by dividing curve by data points in (a).

high recoil-proton momenta, Pauli-exclusion-principle effects, and losses due to momentum transfers resulting in zero-range protons.³ Furthermore, the use¹⁸ of *absolute* detection and scanning efficiencies is avoided. Finally, consistent results obtained from three independent samples (0γ , 1γ , and 2γ events) greatly fortify this approach.

Systematic errors are possible if spectator cuts are made¹⁷ and backgrounds exist such that N and N_6 in Eq. (7) are affected differently. We made no such cuts. Further study^{1d} of other possible systematic errors led to the conclusion that under reasonable assumptions^{10, 16, 19} those errors should be cumulatively less than 10%.

As a check on our results, we calculated our pathlength using the formula $P = \frac{1}{2} A \rho L N$, where A = Avogadro's number, ρ = deuterium density, L = interaction length, and N = number of beam tracks.¹⁸ The data in Table I then yield 5.62 events/ μb for the exposure as a whole. For comparison, Moore,⁴ looking for strange particles in the same film, obtained 5.33 events/ μb . Correcting for unseen spectators (2.33 ± 0.18) and using a 2-prong scan-measuring efficiency of 75%,^{1d} we

obtained $P = 1.81 \pm 0.20$ events/ μb , in good agreement with the other method.

III. METHOD

After a preliminary consideration of the data^{1b} we extracted the $2\pi^0$ spectrum in three ways. First, we fitted our experimental $(MM)^2$ distributions to a model incorporating resonance, $2\pi^0$, and $3\pi^0$ production. Secondly, we performed a detailed background subtraction using background estimates obtained in several independent ways. Finally, we used our γ information by kinematically fitting the sample with two or more observed photons to a $2\pi^0$ hypothesis.

A. Model Fitting

We have fitted²⁰ our mass spectra to a model of the form

$$N_i \propto N_\pi (f_{\text{BW}})_\pi + N_\eta (f_{\text{BW}})_\eta + N_\omega (f_{\text{BW}})_\omega + N_{2\pi} (f_{\text{PS}})_{2\pi} + N_{3\pi} (f_{\text{PS}})_{3\pi}, \quad (8)$$

where N_i is the number of events in the i th mass bin, and N_π , N_η , N_ω , $N_{2\pi}$, and $N_{3\pi}$ are the numbers of π^0 , η , ω , $2\pi^0$, and $3\pi^0$'s in each plot to be obtained from the fit. f_{BW} is a simple Breit-Wigner shape of the form

$$(f_{\text{BW}})_x \propto \frac{1}{[(MM)^2 - M_x^2]^2 + (\frac{1}{2}\Gamma_x)^2}, \quad (9)$$

and f_{PS} is the appropriate phase space obtained from FAKE. We find^{1d} that a Breit-Wigner shape better approximates our resolution function than a Gaussian. Tables III and IV give the input and output parameters for these fits.

We have also attempted fits to the spectrum assuming (1) only $2\pi^0$ phase space, and (2) only $3\pi^0$ phase space. The resulting χ^2 values were about 3–4 times greater than those in Table IV. This is unacceptably high.

We conclude from the excellent fits obtained that our model provides a good representation of our data. The rather low $3\pi^0$ background indicated in Table IV (23% for $t < 15\mu^2$) confirms the indications of the preliminary examination of the data.^{1d}

TABLE III. Breit-Wigner (BW) shape parameters.

| | M^2 [(GeV/c) ²] | $\frac{1}{2}\Gamma$ (GeV/c ²) |
|----------|-------------------------------|---|
| π^0 | 0.0182 ± 0.0027 | 0.0323 ± 0.0025 |
| η | 0.305 ± 0.004 | 0.0418 ± 0.0072 |
| ω | 0.605 ± 0.012 | 0.0537 ± 0.036 |

TABLE IV. Model-fitting results (No. of events).

| Cuts | N_{π^0} | N_{η} | N_{ω} | $N_{2\pi^0}$ | $N_{3\pi^0}$ | $\chi^2/d.f.$ ^a |
|--------------------|-------------|------------|--------------|--------------|--------------|----------------------------|
| none | 688 ± 32 | 417 ± 45 | 172 ± 39 | 995 ± 127 | 450 ± 79 | 77/61 |
| $t < 15\mu^2$ | 445 ± 23 | 153 ± 26 | 70 ± 23 | 574 ± 72 | 176 ± 43 | 57/61 |
| $\cos\theta > 0.8$ | 434 ± 23 | 140 ± 25 | 54 ± 23 | 564 ± 80 | 178 ± 45 | 65/61 |

^aDegrees of freedom.

B. Background Subtraction

We have also made independent estimates for each of the background channels in reaction (3) and subtracted them to obtain a clean $2\pi^0$ spectrum. This method has been used by Smith and Manning¹⁷ in a missing-mass experiment also in deuterium. We discuss each background estimate in turn and display the result in Fig. 7.

1. $\pi^+n \rightarrow \pi^0p$

Because of the rather poor experimental resolution, the π^0 tail extends into the $2\pi^0$ threshold region. Examination of the data suggested that the wings of the resolution function at the π^0 mass is best represented by a shape 50% Breit-Wigner and 50% Gaussian.^{1d} Such a shape was used to estimate the π^0 tail.

2. $\pi^+n \rightarrow p\eta^0, \omega^0$

The η and ω subtractions could not be done on an event-by-event basis because the film was only partially scanned for multiprong events. We used our 3- and 4-prong samples⁵ to obtain the ratio of η/ω production, the published ω -production cross section^{3, 10, 21, 22} and branching ratios,²³ and

our pathlength (1.74 events/ μ b) to obtain these estimates. We also used the angular distributions from our 3- and 4-prong events.⁵

3. $\pi^+n \rightarrow p\eta'(958)$

A simple estimate was made using Rader's¹⁹ results. His cross section of $104 \pm 24 \mu$ b is in agreement with our own determination of $121 \pm 59 \mu$ b based on the neutral mode.^{1d}

4. $\pi^+n \rightarrow p3\pi^0$

The $3\pi^0$ cross section was measured by Crouch *et al.*¹⁵ in hydrogen. They obtained a value for the ratio

$$r_{3\pi^0} = \frac{N(3\pi^0)}{N(2\pi^0) + N(3\pi^0)} \quad (10)$$

of 0.20 over the entire Chew-Low plane. Here N is the number of $3\pi^0$ ($2\pi^0$) events excluding $\eta \rightarrow 3\pi^0$ (but including Δ production). However, since we observe only part of the Chew-Low plane, we regarded that result as merely a useful guide to the general $3\pi^0$ background level, and expended some effort to obtain independent values for $r_{3\pi^0}$, especially for low t . Three techniques were used. The first estimate was obtained from the model-fitting results. Next, relative detection efficiencies were used. Finally, we were able to estimate $r_{3\pi^0}$ from the kinematic fitting procedure sketched previously and to be discussed further in Sec. III C. Our values for $r_{3\pi^0}$ and the values actually used are summarized in Table V.

5. $\pi^+n \rightarrow \pi^0\Delta^+(1236)$

Our last source of contamination, that due to dipions originating from $\Delta^+(1236)$ production, was investigated in the following three ways.^{1d} First, the results of previous studies²⁴⁻²⁷ and charge independence suggest $r_{\Delta^+} \lesssim 20\%$. Second, the highly peripheral nature of the Δ^+ production mechanism should be reflected in a sharp peaking of the 2γ opening angle distribution at small angles if Δ^+ production is large. No such peaking is observed. Finally, our $2\pi^0$ fits give the Δ^+ production level indicated on Fig. 8. We used the values given in Table VI. These numbers are in disagreement

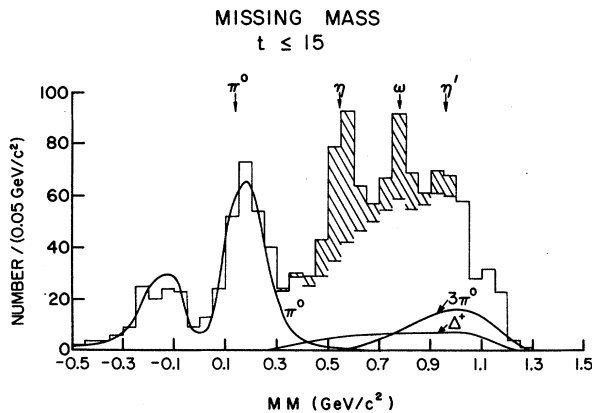


FIG. 7. Illustration of subtraction method showing background subtractions. Shaded area represents η , ω , and η' subtractions. Curve on left shows π^0 subtraction. The $3\pi^0$ and Δ^+ background levels are also indicated. t is the momentum transfer in units of μ^2 .

TABLE V. $3\pi^0$ background estimates.

| $r_{3\pi}$ for | Model fitting | Det. eff. | γ fits | Mean | Used |
|----------------|-----------------|-----------------|-----------------|-----------------|-----------------|
| no cut | 0.31 ± 0.06 | 0.25 ± 0.23 | 0.37 ± 0.12 | 0.30 ± 0.14 | 0.30 ± 0.05 |
| $t < 15\mu^2$ | 0.23 ± 0.06 | 0.07 ± 0.23 | 0.12 ± 0.15 | 0.14 ± 0.14 | 0.17 ± 0.05 |

with those obtained¹⁷ from Corbett *et al.*'s data ($r_{\Delta} = 0.4$ for both cases), but are consistent with Bensinger's¹⁸ ($\approx 10\%$).

C. γ Fitting

The third technique used to extract an enriched sample of $2\pi^0$ events from our data made direct use of the γ information contained in our 2-, 3-, and 4- γ samples by fitting those events to $2\pi^0$ hypotheses. All results presented here are based on fits to the 2γ sample.

The confidence-level distributions for events fitting either of the $2\pi^0$ hypotheses are shown in Figs. 9(c) and 9(d). Since the constraint class is determined on the basis of minimum-opening-angle considerations, the meaning of these distributions is not clear. They differ considerably from the

generally flat distributions we observe for our normal 1-C and 2-C fits. To interpret these distributions, we processed, separately, FAKE $2\pi^0$'s and $3\pi^0$'s with the same fitting program. In Figs. 9(a) and 9(b) we present the FAKE confidence-level distributions. $2\pi^0$'s from Δ^+ production look like "pure" $2\pi^0$'s. Noting the different character of these distributions for $2\pi^0$'s and $3\pi^0$'s, we conclude that a confidence-level cut of ~ 0.2 should considerably suppress the $3\pi^0$ channel. Next, we fitted these curves to our data. Assuming that only $2\pi^0$'s and $3\pi^0$'s remain, the results of these least-squares fits — the curves in Figs. 9(c) and 9(d) — allowed us to obtain the $3\pi^0$ background estimates mentioned above.

Accepting only those events with confidence levels ≥ 0.2 , we estimate, after small π^0 , η , and ω subtractions ($\sim 15\%$), that the resulting sample is 16% contaminated with $3\pi^0$'s. The last number is 9% for $t < 15\mu^2$. The $2\pi^0$ distributions resulting from this technique are presented in Sec. IV.

To convince ourselves of the efficacy of this procedure, we plotted Fig. 10. Here the 2γ sample is divided into two classes: "Fits" are events with confidence level ≥ 0.2 and "nonfits" include everything else above the η mass. The excellent agreement of both mass and momentum-transfer distributions with FAKE predictions proves that this method works.

IV. RESULTS

We now summarize the pertinent results of the above approaches, making comparison with data available from other $2\pi^0$ experiments whenever possible. We point out that our final cross sections are reduced relative to our previously reported^{1a} results which were based on the statistically smaller 2γ sample.

A. Production Cross Sections

Cross sections for reaction (1), obtained from the three methods discussed above, are displayed

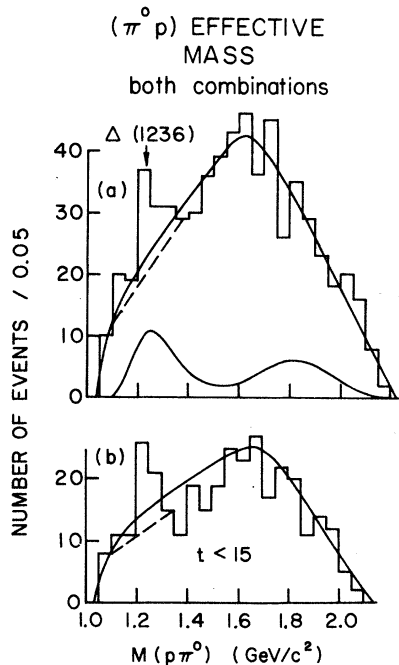


FIG. 8. $\pi^0 p$ effective mass plots showing $\Delta^+(1236)$ contribution to $2\pi^0$ final state. The 2γ sample was fit to $2\pi^0$ hypotheses based on minimum-opening-angle considerations. (a) No t cut. Upper (lower) curve was obtained from FAKE $2\pi^0$ (Δ^+) events run through SQUAW. Events above dashed line were used in Δ^+ background estimate. (b) Same as (a) but for $t < 15$, in units of μ^2 .

TABLE VI. Δ^+ background estimates.

| | No t cut | $t < 15\mu^2$ |
|--------------|-----------------|-----------------|
| r_{Δ} | 0.18 ± 0.05 | 0.16 ± 0.05 |

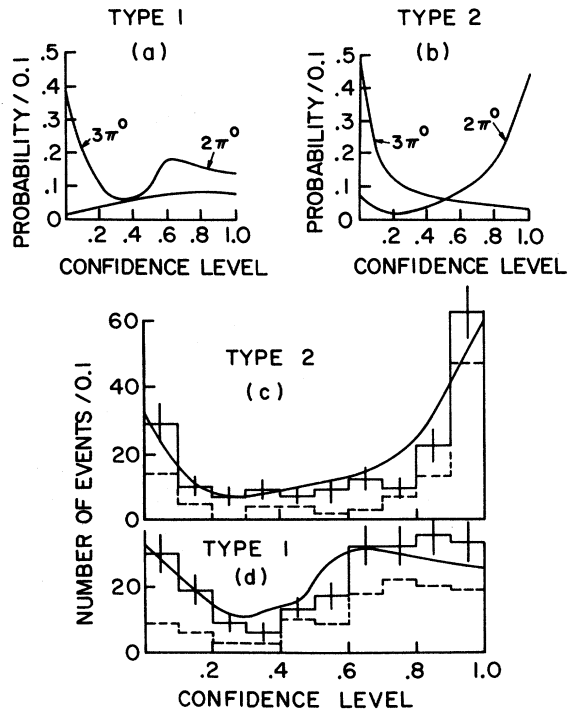


FIG. 9. Confidence-level distributions from SQUAW for 2γ events. (a) For FAKE-generated $2\pi^0$ and $3\pi^0$ events best fitting the $2\pi^0$ hypothesis where both γ 's come from one π^0 ; (b) same as (a) but for events best fitting the $2\pi^0$ hypothesis for which one γ comes from each π^0 . (c) For experimental data with (dashed) and without t cut, $t < 15\mu^2$, for type-2 $2\pi^0$ hypothesis. Curve is best fit of shapes in (b) to uncut data. (d) Same as (c) but for type-1 $2\pi^0$ hypothesis.

in Table VII. The results are seen to be quite consistent.

For comparison, we present in Table VIII the results of some other $2\pi^0$ experiments.^{15, 17, 18, 28} The center-of-mass energy is ~ 2.2 GeV/ c^2 in each case.

B. Mass Spectra

The results of Sec. III are shown in Figs. 11–14. These mass plots are consistent in both shape and magnitude.

In Fig. 15 we compare our $2\pi^0$ spectrum with those of other experiments.^{17, 18, 28} The most important feature of this plot is that all four experiments yield similar shapes for the $2\pi^0$ spectrum consistent with phase space and with no evidence for any relatively narrow resonances.^{1b} There is disagreement in magnitude with the results of Ref. 28.

C. Other Distributions

In Fig. 16 we compare our t distribution with that of Bensinger¹⁸ and note good agreement. We

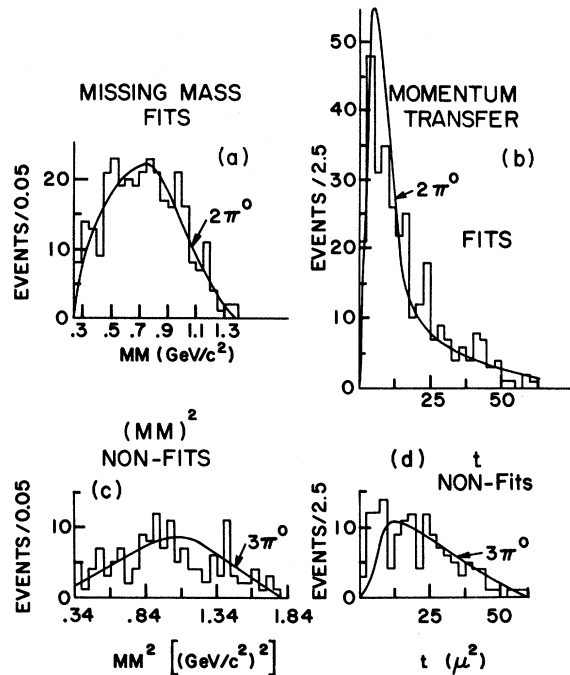


FIG. 10. Results of γ -fitting procedure, showing that this procedure is useful in suppressing $3\pi^0$ background. (a) and (b) are MM and t distributions for events best fitting either one of the $2\pi^0$ hypotheses with a confidence level ≥ 0.2 . (c) and (d) are for events not accepted as $2\pi^0$ fits by the program. The $2\pi^0$ and $3\pi^0$ curves were obtained from FAKE events.

also indicate the corresponding distribution from the $\pi^+\pi^-$ data of West *et al.*²⁴ normalized to our peak ($t < 10\mu^2$). The close agreement of these plots suggests similarities in the two production processes.

We define the $\pi\pi$ scattering angle as the angle in the dipion center of mass between a π^0 and the beam particle. In Fig. 17 we show the distribution of the cosine of this angle for some mass ranges for “ $2\pi^0$ fits” from the 2γ sample. No corrections for residual background have been applied. These distributions are consistent with isotropy indicating dominant s -wave decay of the $2\pi^0$ system and a small amount of d wave in the upper mass range, in agreement with Bensinger's results.¹⁸

TABLE VII. Cross sections for $\pi^+n \rightarrow p\pi^0\pi^0$ in μb .

| | (1) Model | (2) Subtraction | (3) γ fits | Mean |
|--------------------|--------------|--------------------|----------------------|--------------|
| Scan cut | 708 \pm 96 | 629 \pm 70 | 616 \pm 78 | 651 \pm 47 |
| $t < 15\mu^2$ | 411 \pm 56 | 380 \pm 42 | 368 \pm 55 | 386 \pm 30 |
| $\cos\theta > 0.8$ | 421 \pm 64 | 400 \pm 44 | 384 \pm 55 | 402 \pm 32 |

TABLE VIII. Comparisons of $2\pi^0$ cross sections in μb .

| Cuts | Ref. | 17 | 18 | 15 | 28 | This exp't |
|--------------------|------|----------------|----------------|-----------------|----------------|----------------|
| None | | | 825 ± 101 | 1290 ± 80^a | 590 ± 90^a | |
| Scan cut | | | 570 ± 67^b | | | 651 ± 47^c |
| $t < 15\mu^2$ | | | 379 ± 46 | | | 386 ± 30 |
| $\cos\theta > 0.8$ | | 293.6 ± 30 | | | 116 ± 14 | 402 ± 32 |

^a $\Delta(1236)$ included.
^b $p < 1 \text{ GeV}/c$.
^c $p < 1.25 \text{ GeV}/c$.

According to OPE, $d\sigma/dMdt$ should fall as $1/p^2$ with increasing beam momentum. Our results confirm that dependence. This is shown in Fig. 18 where we have added our data points to those of Sonderegger and Bonamy.²⁹

V. $\pi\pi$ INTERACTIONS

Assuming that a Feynman OPE diagram represents the dominant process contributing to reac-

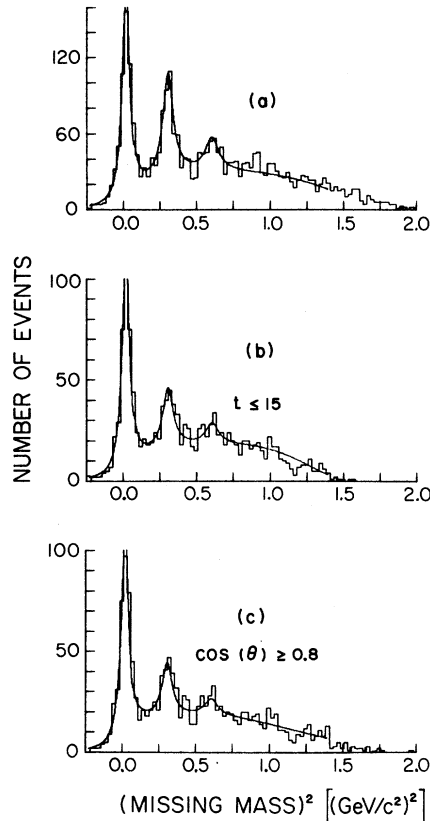


FIG. 11. Fits of model to MM^2 distributions. (a) No cuts. (b) $t < 15$. t is momentum transfer in units of μ^2 . μ is pion mass. (c) c.m. production cosine $\cos(\theta) > 0.8$.

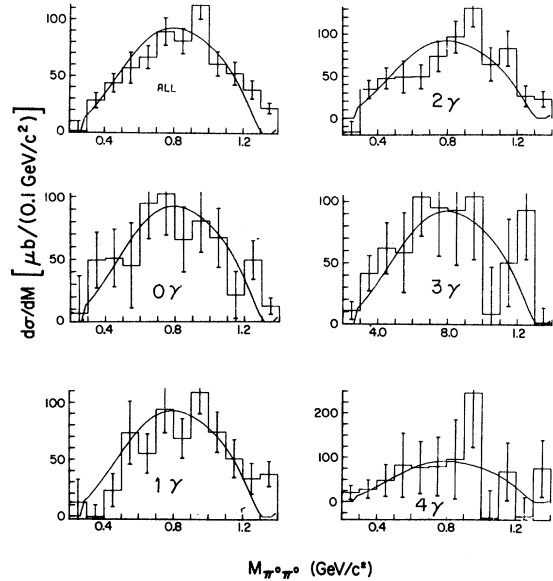


FIG. 12. Subtraction-method-derived $2\pi^0$ mass spectra for each sample and all combined, without t cut. Each phase-space curve has the same area. No $\eta(960)$ corrections have been made.

tion (1), we are then able to show that only one set of s -wave phase shifts, the so-called up-down solution, explains our and similar data below $M_{\pi\pi} = 1 \text{ GeV}/c^2$. As usual, only elastic s - and p -wave scattering is considered.

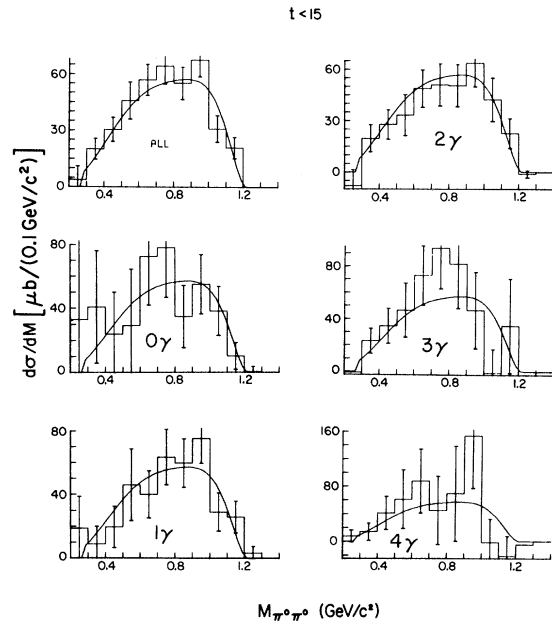


FIG. 13. Same as Fig. 12 except that $t < 15$. t is in units of μ^2 .

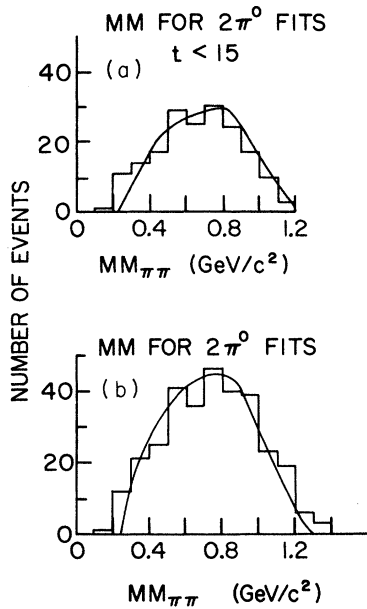


FIG. 14. $2\pi^0$ kinematic fitting results. Missing-mass distribution for (a) Events accepted as $2\pi^0$ fits, momentum transfer $t < 15$, in units of μ^2 . (b) Same as (a) for no t cut. No cut has been made to exclude Δ^+ production.

A. Total-Cross-Section Determination

The Chew-Low formula relates the total $\pi\pi$ cross section σ and the differential pion-production cross section $d^2\sigma/dMdt$.³⁰ Various approaches are possible in reaching the limit of that equation. We

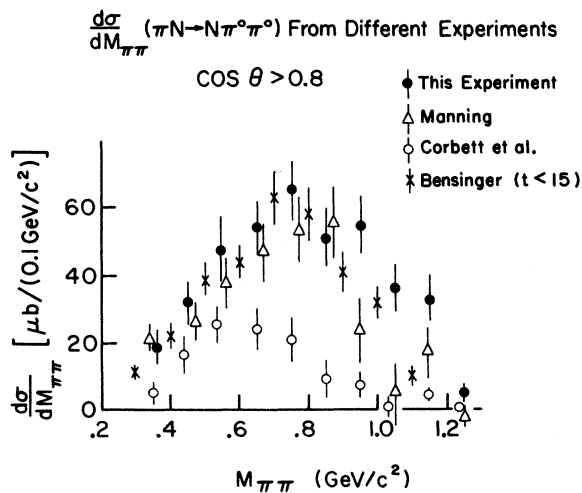


FIG. 15. Comparison of our $2\pi^0$ mass plot from subtraction method with those of Refs. 17, 18, and 28. Bensinger's (Ref. 18) result is for momentum transfers $t < 15 \mu^2$.

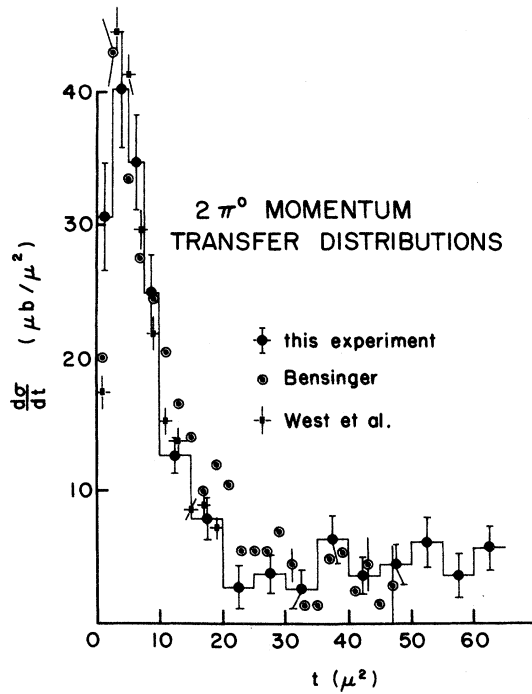


FIG. 16. Momentum-transfer distributions compared. West's (Ref. 24) data are for $\pi^-p \rightarrow \pi^+\pi^-n$, normalized to our peak ($t < 10$).

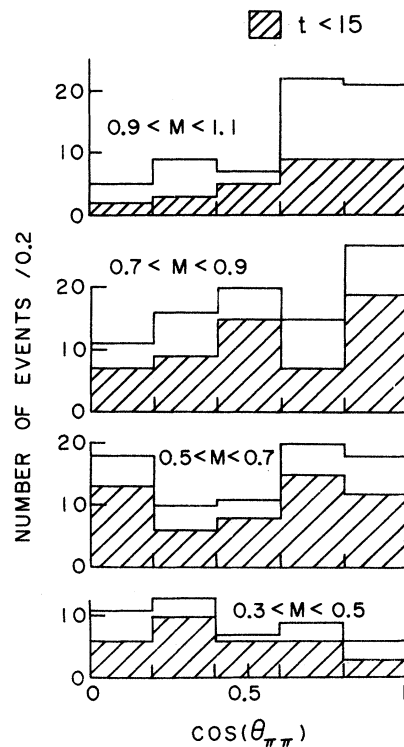


FIG. 17. $\pi\pi$ scattering-angle distributions as a function of dipion mass.

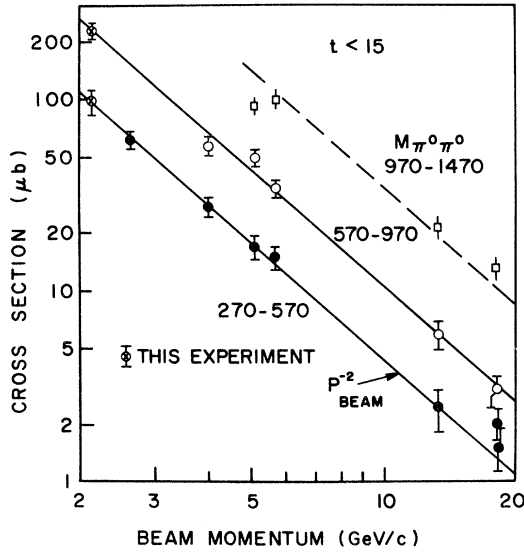


FIG. 18. $d\sigma/dMdt$ for the $2\pi^0$ channel as a function of the beam momentum [taken from Sonderegger and Bonamy (Ref. 29)]. Our data points are for $0.3 < M_{2\pi^0} < 0.6$ and $0.6 < M_{2\pi^0} < 0.9$ GeV/c^2 .

have applied the extrapolation³¹ and form-factor techniques¹⁸ to our data and obtained agreement within error. Our results are compared to some other experiments in Fig. 19.^{18, 29, 32}

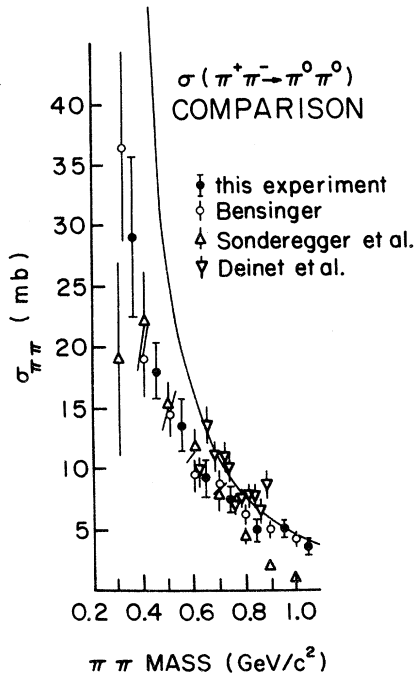


FIG. 19. $\pi\pi$ cross sections from different experiments (Ref. 18, 29, 32).

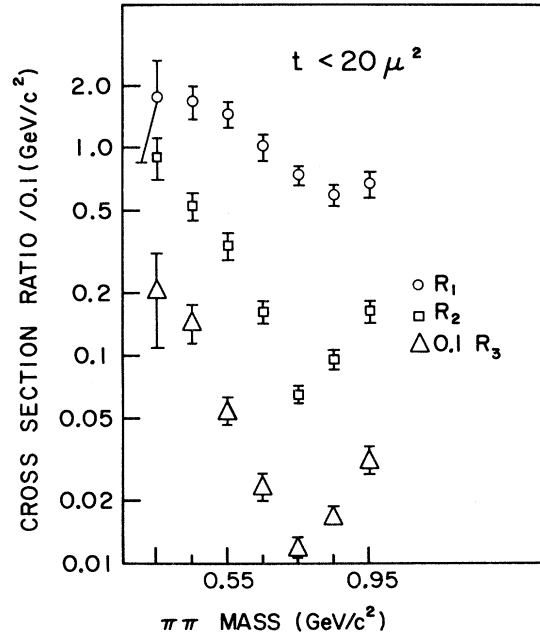


FIG. 20. Experimental ratios R_1 , R_2 , and R_3 for $t < 20$ vs $\pi\pi$ effective mass.

B. δ_0 Determination

Ambiguities in δ_0 , the dipion s -wave $I=0$ scattering phase, and the relative sensitivity of the s - p wave interference analyses³³ to absorptive corrections leads one to consider other ways of analyzing the data. The measurement of the $\pi^+n \rightarrow p\pi^0\pi^0$ cross section has made possible the combination of pion-production data in such a way as to provide a unique determination of δ_0 and other $\pi\pi$ scattering parameters with minimal assumptions.

Our method consists of forming three independent ratios of four single-pion production cross

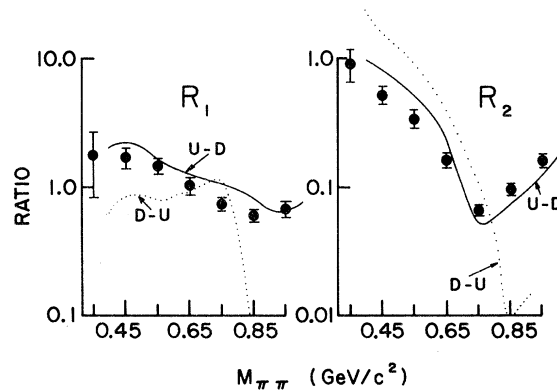


FIG. 21. Comparison of experimentally determined R_1 and R_2 with predictions of Malamud and Schlein's analysis (Ref. 31).

sections and relating the resulting ratios to the $\pi\pi$ scattering phase shifts via the Chew-Low formula. Thus, if pion exchange dominates at low momentum transfers to the final-state nucleon, we have^{1d}

$$\begin{aligned}
 R_1 &= \frac{d\sigma}{dMdt}(\pi^-p \rightarrow \pi^0\pi^0n) \Big/ \frac{d\sigma}{dMdt}(\pi^+p \rightarrow \pi^+\pi^+n) = \frac{1}{9} \frac{\sin^2\delta_0 + \sin^2\delta_2 - 2\sin\delta_0\sin\delta_2\cos(\delta_0 - \delta_2)}{\sin^2\delta_2}, \\
 R_2 &= \frac{d\sigma}{dMdt}(\pi^-p \rightarrow \pi^0\pi^0n) \Big/ \frac{d\sigma}{dMdt}(\pi^-p \rightarrow \pi^-\pi^+n) \\
 &= \frac{1}{2} \frac{\sin^2\delta_0 + \sin^2\delta_2 - 2\sin\delta_0\sin\delta_2\cos(\delta_0 - \delta_2)}{\sin^2\delta_0 + \frac{1}{4}\sin^2\delta_2 + \sin\delta_0\sin\delta_2\cos(\delta_0 - \delta_2) + \frac{3}{4}X\sin^2\delta_1}, \\
 R_3 &= \frac{d\sigma}{dMdt}(\pi^-p \rightarrow \pi^0\pi^0n) \Big/ \frac{d\sigma}{dMdt}(\pi^-p \rightarrow \pi^-\pi^0p) \\
 &= \frac{4}{9} \frac{\sin^2\delta_0 + \sin^2\delta_2 - 2\sin\delta_0\sin\delta_2\cos(\delta_0 - \delta_2)}{\sin^2\delta_2 + 3X\sin^2\delta_1},
 \end{aligned} \tag{11}$$

where δ_2 and δ_1 are the $I=2$, $l=0$ and $I=1$, $l=1$ phase shifts. The factor X is included to describe relative deviations of s - and p -wave scattering from the on-shell case. Absorbing X into the p -wave phase shift, R_1 , R_2 , and R_3 then represent three equations to be solved for three unknowns. Our experimental ratios are shown in Fig. 20.

In Fig. 21³¹ we compare our experimentally determined R_1 and R_2 with the predictions of the moment analysis of Malamud and Schlein.³¹ The

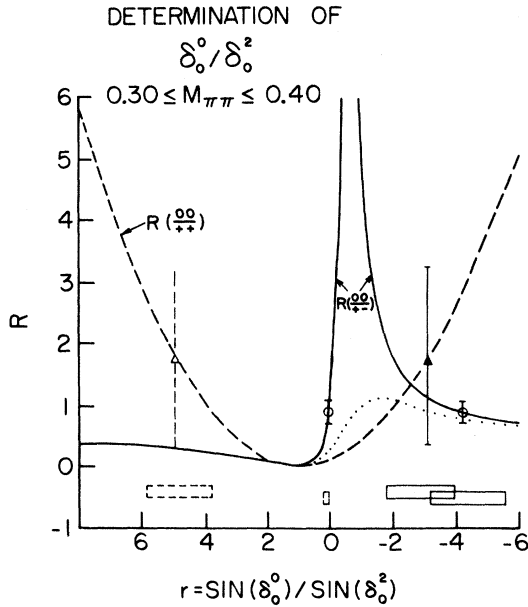


FIG. 22. Determination of the average value of δ_0/δ_2 (denoted δ_0^0/δ_2^2 in the figure) in the threshold region. The dashed (full) curve is the theoretical value of R_1 (R_2) as a function of $r = \delta_0/\delta_2$ for $\delta_2 = -6^\circ$ and $\delta_1 = 0.8^\circ$. The values of r allowed by the experimental R 's for $t < 20\mu^2$ are shown by the rectangles along the abscissa. The dotted curve shows R_2 for $\delta_1 = 3^\circ$ and indicates the effect of absorption.

up-down solution is clearly preferred by the data.³⁵ Thus, our experimental ratios resolve the four-fold ambiguity of other analyses. Also, the fact that the same set of phase shifts describes both independent pieces of data reasonably well provides support for the OPE model.

Regarding the $\pi\pi$ threshold region, we showed earlier^{1c} how R_1 and R_2 may be used to obtain the ratios $r = \delta_0/\delta_2 = a_0/a_2$, where the a 's are the s -wave $\pi\pi$ scattering lengths. We have redone that analysis using additional data.^{1d} Our final solution is shown in Fig. 22 which yields the results

$$\delta_0/\delta_2 = a_0/a_2 = -(3.2^{+1.5}_{-1.0})$$

in good agreement with our earlier results and other determinations.³⁰ Using Olsson's calculation,³⁶ $2a_0 - 5a_2 = (0.52 \pm 0.05)\mu^{-1}$, we then obtain

$$a_0 = +(0.15 \pm 0.08)\mu^{-1},$$

$$a_2 = -(0.05 \pm 0.01)\mu^{-1}.$$

a_0 is consistent with the measurement of Maung *et al.*,³⁷

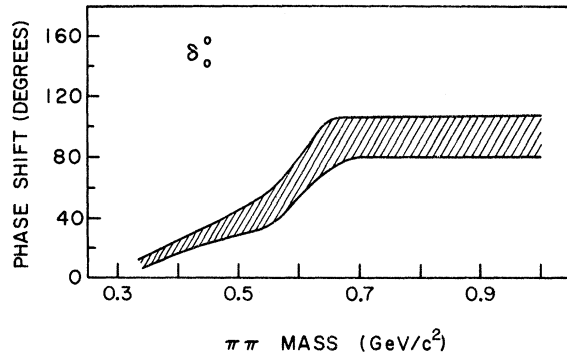


FIG. 23. Determination of $I=0$ s -wave $\pi\pi$ phase shift from this experiment using the three independent cross-section ratios R_1 , R_2 , and R_3 given in Fig. 20.

current-algebra predictions,^{1c} and preliminary indications from the recent K_{e4} data.³⁸

Finally, we used Eqs. (11) to obtain δ_0 for $M_{\pi\pi} < 1 \text{ GeV}/c^2$.^{1d} Since δ_2 is fairly well known, we used an average of available data in our analysis. That implies three transcendental equations to be solved for two unknowns. We made a graphical analysis similar to that used in Fig. 22 to determine a consistent set of δ_0 . Using the fact that most other analyses agree that $\delta_0 > 60^\circ$ in the range $0.7 < M_{\pi\pi} < 1 \text{ GeV}/c^2$, we obtained the $l=0$, $l=0$ phase shifts shown in Fig. 23. In an attempt to interpret the factor X in Eqs. (1b) and (1c), we used a p -wave Breit-Wigner shape for δ_1 ($M_\rho=765$, $\Gamma_\rho=150$). The resulting behavior of X was found

to be entirely consistent with that indicated by the absorption-model calculations of Bander *et al.*³⁴

ACKNOWLEDGMENTS

We wish to thank everyone who helped bring this work to completion. Our thanks go to the ZGS and 30-in. bubble chamber crews, the Wisconsin scanning and measuring staff, and the Madison Academic Computing Center. In particular, we are indebted to Mrs. Betty Foley for her patient editing job and to Vic Scherer for his considerable help and cooperation. One of us (KJB) would like to thank Professor W. F. Fry for his support and encouragement.

*Division of Physical Oceanography RSMAS, University of Miami, 10 Rickenbacker Causeway, Miami, Florida 33149.

- ¹(a) K. J. Braun, D. B. Cline and V. Scherer, *Phys. Rev. Lett.* **21**, 1275 (1968). (b) D. B. Cline, K. J. Braun and V. Scherer, in *Proceedings of the Conference on $\pi\pi$ and $K\pi$ Interactions*, Argonne National Laboratory, 1969, edited by F. Loeffler and E. D. Malamud (Argonne National Laboratory, Argonne, Ill., 1969), p. 179. (c) D. Cline, K. J. Braun, and V. Scherer, *Nucl. Phys.* **B18**, 77 (1970). (d) K. J. Braun, Ph.D. thesis, University of Wisconsin, Madison, 1972 (unpublished).
- ²(a) C. Goebel, *Phys. Rev. Lett.* **1**, 337 (1958). (b) G. F. Chew and F. E. Low, *Phys. Rev.* **113**, 1640 (1959).
- ³R. J. Miller, S. Lichtman, and R. B. Willmann, Purdue University Report No. C00-1428-93 (unpublished).
- ⁴C. Moore, Ph.D. thesis, University of Wisconsin, 1970 (unpublished).
- ⁵V. Scherer, private communication. The 3- and 4-prong data in this film were partially analyzed, i.e., $\pi^+d \rightarrow p(p)\pi^+\pi^-\pi^0$, $p(p)\pi^+\pi^-$.
- ⁶M. A. Abolins, O. I. Dahl, J. S. Danburg, D. Davies, P. Hoch, J. Kirz, D. H. Miller, and R. Rader, paper submitted to Heidelberg International Conference on Elementary Particles, Heidelberg, Germany, 1967 (unpublished).
- ⁷(a) DIANA, written by R. W. Hartung, was combined with HASH, written by R. H. March, into a reconstruction-fitting program. (b) O. I. Dahl, T. B. Day, and F. T. Solmitz, Alvarez Group Programming Note No. P-126, 1965 (unpublished). We are indebted to T. Carroll for providing us with his version of SQUAW.
- ⁸(a) R. M. Morse, Ph.D. thesis, University of Wisconsin, Madison, 1969 (unpublished). (b) T. Carroll, Ph.D. thesis, University of Wisconsin, Madison, 1971 (unpublished).
- ⁹(a) Program FAKE was written by G. Lynch, LBL Report No. UCRL-10335 (unpublished). We wish to thank F. Beck for providing us with the ANL version. (b) D. Dekkers *et al.*, *Phys. Lett.* **11**, 161 (1964).
- ¹⁰J. Danburg, M. A. Abolins, O. I. Dahl, D. W. Davies, P. L. Hoch, J. Kirz, D. H. Miller, and R. K. Rader, Lawrence Berkeley Laboratory Report No. UCRL-19272, 1970 (unpublished).
- ¹¹A. S. Carroll, I. F. Corbett, C. J. S. Damerell, N. Middlemas, D. Newton, A. B. Clegg, and W. S. C. Williams, *Phys. Rev. Lett.* **16**, 288 (1966).
- ¹²D. F. Crawford and H. Messel, *Phys. Rev.* **128**, 2352 (1962).
- ¹³A. S. Carroll, I. F. Corbett, C. J. S. Damerell, N. Middlemas, D. Newton, A. B. Clegg, and W. S. C. Williams, *Phys. Rev.* **177**, 2047 (1969).
- ¹⁴(a) V. V. Barmin, A. G. Dolgolenko, A. G. Meshkovsky, and V. A. Shebanov, *Phys. Lett.* **24B**, 249 (1967). (b) J. Alitti *et al.*, *Phys. Lett.* **21**, 354 (1966).
- ¹⁵(a) H. R. Crouch *et al.*, *Phys. Rev. Lett.* **21**, 845 (1968). (b) H. R. Crouch *et al.*, *Phys. Rev. Lett.* **21**, 849 (1968).
- ¹⁶G. C. Benson, Ph.D. thesis, University of Michigan, Ann Arbor, 1966 (unpublished).
- ¹⁷R. J. Manning, Ph.D. thesis, University of California, Berkeley, LBL Report No. UCRL-19339, 1969 (unpublished).
- ¹⁸(a) J. R. Bensinger, Ph.D. thesis, University of Wisconsin, Madison, 1970 (unpublished). (b) J. R. Bensinger, A. R. Erwin, M. A. Thompson, and W. D. Walker, *Phys. Lett.* **36B**, 134 (1971).
- ¹⁹R. K. Rader, Ph.D. thesis, University of California, Berkeley, LBL Report No. UCRL-1943, 1969 (unpublished).
- ²⁰Madison Academic Computing Center (MACC) least-squares fitting program GASAUS.
- ²¹J. H. Boyd, A. R. Erwin, W. D. Walker, and E. West, *Phys. Rev.* **166**, 1458 (1968).
- ²²T. C. Bacon, W. J. Fickinger, D. G. Hill, H. W. K. Hopkins, D. K. Robinson, and E. O. Salant, *Phys. Rev.* **157**, 1263 (1967).
- ²³Particle Data Group, *Rev. Mod. Phys.* **43**, S1 (1971).
- ²⁴E. West, J. H. Boyd, A. R. Erwin, and W. D. Walker, *Phys. Rev.* **149**, 1089 (1966).
- ²⁵B. G. Reynolds, J. R. Albright, R. H. Bradley, E. B. Brucher, B. C. Harms, W. C. Harrison, J. D. Kimel, J. E. Lannutti, W. H. Sims, and R. P. Wieckowicz,

- Phys. Rev. **184**, 1424 (1969).
- ²⁶L. D. Jacobs, Ph.D. thesis, University of California, Berkeley, LBL Report No. UCRL-16877, 1966 (unpublished).
- ²⁷(a) F. E. James and H. L. Kraybill, Phys. Rev. **142**, 896 (1966). (b) A. Benvenuti, Ph.D. thesis, University of Minnesota, Minneapolis, 1969 (unpublished).
- ²⁸I. F. Corbett *et al.*, Phys. Rev. **156**, 1451 (1967). See also Ref. 13.
- ²⁹P. Sonderegger and P. Bonamy, paper submitted to the Fifth International Conference on High Energy Physics, Lund, Sweden, 1969 (unpublished).
- ³⁰J. L. Petersen, Phys. Rep. **2C**, 155 (1971).
- ³¹(a) P. E. Schlein, Phys. Rev. Lett. **19**, 1052 (1967). (b) E. Malamud and P. Schlein, Phys. Rev. Lett. **19**, 1056 (1967).
- ³²W. Deinet, A. Menzione, H. Müller, H. M. Staudenmaier, S. Buniatov, and D. Schmitt, paper submitted to the Fifth International Conference on High Energy Physics, Lund, Sweden, 1969 (unpublished). See also W. Deinet *et al.*, Phys. Lett. **30B**, 359 (1969).
- ³³L. J. Gutay, Purdue University Report No. COD-1428-126, 1969 (unpublished). This paper also appears in *Proceedings of the Conference on $\pi\pi$ and $K\pi$ Interactions, Argonne National Laboratory, 1969*, edited by F. Loeffler and E. D. Malamud (Ref. 1), p. 241.
- ³⁴M. Bander, G. L. Shaw, and J. R. Fulco, Phys. Rev. **168**, 1679 (1968).
- ³⁵Since first submitting this manuscript to the publisher, a paper by M. R. Pennington and S. D. Protopescu, Phys. Rev. D **7**, 1429 (1973), has come to our attention. This paper deals with the resolution of the $\pi\pi$ phase-shift ambiguities and is in agreement with our results.
- ³⁶M. G. Olsson, Wisconsin report, 1969 (unpublished).
- ³⁷T. Maung, G. E. Masek, E. Miller, H. Ruderman, W. Vernon, K. M. Crowe, and N. T. Dairiki, Phys. Lett. **33B**, 521 (1970).
- ³⁸A. Mann, private communication.

PHYSICAL REVIEW D

VOLUME 8, NUMBER 11

1 DECEMBER 1973

Search for Rare K^+ Decays. II. $K^+ \rightarrow \pi^+ \nu \bar{\nu}$ *†

G. D. Cable

*Enrico Fermi Institute, The University of Chicago, Chicago, Illinois 60637
 and Department of Physics, The University of Arizona, Tucson, Arizona 85721*

R. H. Hildebrand and C. Y. Pang

*Enrico Fermi Institute and Department of Physics,
 The University of Chicago, Chicago, Illinois 60637*

R. Stiening‡

Lawrence Berkeley Laboratory, Berkeley, California 94720

(Received 2 July 1973)

In a counter experiment at the Lawrence Berkeley Laboratory Bevatron we have searched for the process $K^+ \rightarrow \pi^+ \nu \bar{\nu}$ in the kinetic energy interval $60 < T_\pi < 105$ MeV and have found no examples of this decay mode. Combining our data with those of Klems, Hildebrand, and Stiening for the interval $117 < T_\pi < 127$ MeV, we obtain the limit $\Gamma(K^+ \rightarrow \pi^+ \nu \bar{\nu}) < 5.6 \times 10^{-7} \Gamma(K^+ \rightarrow \text{all})$, assuming a (vector) pion spectrum like that for $K^+ \rightarrow \pi^0 e^+ \nu$. Limits are presented for other assumed spectra.

I. INTRODUCTION

Klems, Hildebrand, and Stiening¹ have reported a search for the process

$$K^+ \rightarrow \pi^+ \nu \bar{\nu} \quad (1)$$

using apparatus sensitive to π^+ near the kinematic limit ($T_{\pi^+} = 127$ MeV). We report here an extension of the search to the region $60 < T_{\pi^+} < 105$ MeV. Neither experiment has given evidence for this decay mode. Both may be used to establish a limit for the branching ratio.

Both experiments have used the stopping K^+ beam of the LBL Bevatron, and in both counter tech-

niques have been used to identify $K^+ \rightarrow \pi^+ \mu^+ e^+$ decays, measure the π^+ range, and exclude events with other charged particles or γ rays.

In the second experiment a lead-glass γ detector completely surrounded the kaon stopper. This arrangement allowed us to look for examples of process (1) at pion energies below that for

$$K^+ \rightarrow \pi^+ \pi^0 \quad (2)$$

($T_{\pi^+} = 108$ MeV) without errors due to simulation of (1) by (2) when the π^+ range and the $\pi^+ - \pi^0$ angle were reduced by scattering. The new apparatus and its calibration are described in our report on a concurrent experiment on $K^+ \rightarrow \mu^+ \nu \bar{\nu}$.²